THE JOURNAL OF BIOLOGICAL CHEMISTRY VOL. 289, NO. 6, pp. 3294–3306, February 7, 2014

Molecular Basis of Purinergic Signal Metabolism by Ectonucleotide Pyrophosphatase/Phosphodiesterases 4 and 1 and Implications in Stroke*◆

Received for publication, July 28, 2013, and in revised form, December 9, 2013 Published, JBC Papers in Press, December 12, 2013, DOI 10.1074/jbc.M113.505867

Ronald A. Albright[‡1], Deborah L. Ornstein[§1], Wenxiang Cao[¶], William C. Chang[‡¶], Donna Robert[§], Martin Tehan[‡], Denton Hoyer[‖], Lynn Liu[¶], Paul Stabach[‡2], Guangxiao Yang[‡], Enrique M. De La Cruz[¶], and Demetrios T. Braddock[‡3]

From the [‡]Department of Pathology, Yale University School of Medicine, New Haven, Connecticut 06510, the [§]Department of Pathology, Geisel School of Medicine, Dartmouth University, Hanover, New Hampshire 03755, the [¶]Department of Molecular Biophysics and Biochemistry, Yale University, New Haven, Connecticut 06520, and the [‖]Yale Center for Molecular Discovery, Yale University, West Haven, Connecticut 06516

Background: Nucleotide pyrophosphatase/phosphodiesterases (NPPs) metabolize extracellular purinergic signals.
Results: NPP4 and NPP1 exhibit nearly identical active site geometry but distinct substrate specificity.
Conclusion: A tripartite lysine claw in NPP1 stabilizes ATP in the catalytic pocket. NPP4 lacks this motif and is unable to hydrolyze ATP effectively.
Significance: Understanding NPP4 and NPP1 catalysis enables insight into the pathogenesis of stroke and ectopic bone mineralization.

NPP4 is a type I extracellular membrane protein on brain vascular endothelium inducing platelet aggregation via the hydrolysis of Ap3A, whereas NPP1 is a type II extracellular membrane protein principally present on the surface of chondrocytes that regulates tissue mineralization. To understand the metabolism of purinergic signals resulting in the physiologic activities of the two enzymes, we report the high resolution crystal structure of human NPP4 and explore the molecular basis of its substrate specificity with NPP1. Both enzymes cleave Ap3A, but only NPP1 can hydrolyze ATP. Comparative structural analysis reveals a tripartite lysine claw in NPP1 that stabilizes the terminal phosphate of ATP, whereas the corresponding region of NPP4 contains features that hinder this binding orientation, thereby inhibiting ATP hydrolysis. Furthermore, we show that NPP1 is unable to induce platelet aggregation at physiologic concentrations reported in human blood, but it could stimulate platelet aggregation if localized at low nanomolar concentrations on vascular endothelium. The combined studies expand our understanding of NPP1 and NPP4 substrate specificity and range and provide a rational mechanism by which polymorphisms in NPP1 confer stroke resistance.

Extracellular nucleotides engage in paracrine and autocrine cell signaling by binding purinergic receptors on cell surfaces, resulting in a wide range of physiologic responses, including platelet aggregation (1), bone development and remodeling (2), and endocrinopathies such as diabetes and obesity (3, 4). Purinergic P2X receptors present on cell surfaces are ion channels that bind mainly ATP, whereas P2Y receptors are cell surface G-protein-coupled receptors that interact with a broader range of nucleotides. The concentration of extracellular purine substrates driving purinergic signaling is determined by the release of ectonucleotides via degranulation or cell lysis, the rate of ectonucleotide synthesis, and the catabolism of ectonucleotides by ectoenzymes.

The ectonucleotide pyrophosphatase/phosphodiesterase (NPP)[4] enzymatic family is comprised of extracellular phosphodiesterases, some of which are involved in ectonucleotide catabolism. In humans, the NPP family consists of seven extracellular glycosylated zinc-dependent bimetallo-enzymes that hydrolyze phosphodiester bonds in a variety of substrates, ranging from nucleotides (NPP1 (5), NPP3 (6), and NPP4 (7)) to lipids (NPP2 (8–10), NPP6 (11), and NPP7 (12)). The NPP family is implicated in a variety of pathologic and physiologic processes, including tumor invasion and metastasis (13–16), inflammation (17), lung fibrosis (18) and angiogenesis (NPP2) (19, 20), tissue calcification and bone development (NPP1) (2, 21–23), and hemostasis and platelet aggregation (NPP4) (7). Despite significant catalytic domain sequence homology, the substrate specificity of NPP enzymes varies widely, and details of the molecular determinants of nucleotide substrate specificity remain unclear (24). Here, we focus on NPP4 and NPP1, which target nucleotide-containing substrates.

Platelet aggregation is induced via interaction of extracellular ADP with platelet $P2Y_1$ and $P2Y_{12}$ purinergic receptors, resulting in rapid calcium influx followed by further platelet

* This work is supported by Connecticut Department of Public Health Grant RFP 2013-0913 (to D. T. B.).
◆ This article was selected as a Paper of the Week.
The atomic coordinates and structure factors (codes 4LQY and 4LR2) have been deposited in the Protein Data Bank (http://wwpdb.org/).
[1] Both authors contributed equally to this work.
[2] Present address: MIT Lincoln Laboratory, Group 48 Bioengineering Systems and Technologies, 244 Wood St., Lexington, MA 02420.
[3] To whom correspondence should be addressed: Dept. of Pathology, Yale University School of Medicine, 310 Cedar St., New Haven, CT 06510. Tel.: 203-737-1278; Fax: 203-785-6899; E-mail: demetrios.braddock@yale.edu.

[4] The abbreviations used are: NPP, nucleotide pyrophosphatase/phosphodiesterase; Ap3A, diadenosine triphosphate; PDB, Protein Data Bank; r.m.s.d., root mean square deviation; pNP-TMP, *p*-nitrophenyl 5′-thymidine monophosphate; AP, alkaline phosphatase.

activation, degranulation, and irreversible shape change to extend the growing thrombus (1, 26). Metabolism of extracellular ADP by membrane-bound CD39 on vascular endothelial cells (27–30) and soluble phosphohydrolases in the platelet microenvironment (31–33) rapidly degrades ADP into AMP and P_i, limiting the extension of the aggregatory burst of ADP to platelets in the immediate vicinity of the activated, degranulating platelets. AMP is further metabolized by membrane-bound CD73 into adenosine (34, 35), a potent antithrombotic signaling molecule that modulates vascular tone, decreases leukocyte adhesion, and limits thrombus formation (35). The release of platelet dense core granules disgorges high concentrations of ADP into the thrombotic microenvironment, further stimulating platelet aggregation.

Platelet dense core granules also contain high concentrations of the dinucleotide Ap3A, which can reach local concentrations of over 100 μM upon platelet degranulation (36–39). The role of Ap3A in hemostasis has never been fully defined, but Ap3A has long been thought to represent more stable "chemically masked" ADP that could be released into the thrombotic microenvironment to sustain platelet aggregation (40). Ap3A hydrolytic activity has been identified on the vascular surfaces of both bovine (41) and porcine (42) endothelial cells, and we recently proposed NPP4 as the enzyme responsible for Ap3A hydrolysis to ADP by demonstrating the enzyme to be abundantly present on the surface of human brain vascular endothelium and by showing that nanomolar concentrations of NPP4 promote irreversible platelet aggregation in the presence of physiologic concentrations of Ap3A (7). Our studies suggest that NPP4 promotes hemostasis by providing a sustained source of ADP to a developing thrombus being steadily depleted of ADP by CD39 and soluble phosphohydrolases.

NPP1 (also known as PC-1) is a type II extracellular membrane-bound glycoprotein located on the mineral-depositing matrix vesicles of osteoblasts and chondrocytes. NPP1 catabolizes extracellular ATP into AMP and PP_i (2, 43). PP_i functions as a potent inhibitor of ectopic tissue mineralization by binding to nascent hydroxyapatite (HA) crystals, thereby preventing the future growth of these crystals (2, 44), but increased PP_i concentrations have been shown to promote calcification under certain circumstances (45). Importantly, point mutations that decrease the enzymatic activity of NPP1 are associated with several human diseases of tissue mineralization, including idiopathic infantile arterial calcification (22) and hypophosphatemic rickets (46), and mouse models of impaired NPP1 function (either knock-outs or knock-ins, including so-called tip toe walking (ttw) mice) result in phenotypes that mimic many of the above human diseases (21, 23, 47, 48), including osteoarthritis, exuberant calcification of the posterior spine as seen in ossification of the posterior longitudinal ligament, and calcification of arterial vessels and heart as seen in idiopathic infantile arterial calcification. Recently, polymorphisms in NPP1 have been identified that confer stroke protection in pediatric patients with sickle cell anemia (49).

Both hemostasis and bone development are essential finely balanced physiologic processes that are regulated by the extracellular metabolism of purinergic signals. To better understand the role and atomic details of purinergic signal metabolism by NPP1 and NPP4, we determined the high resolution structure of NPP4, the first human NPP to be solved, and undertook a structural and enzymatic characterization of NPP4 *versus* NPP1. In addition, we directly measured the effect of NPP1 on platelet aggregation in the presence of physiologic levels of Ap3A. We discovered that despite the high degree of sequence identity and homology and shared structural features that allow for the targeting of a mostly similar set of nucleotide-containing substrates, these two enzymes also possess key structural differences that account for the distinct substrate specificities central to their biologic functions. Our studies describe the molecular basis of substrate discrimination by NPP4 and NPP1, provide insight into their physiologic roles governing bone mineralization and platelet aggregation, and provide an apparent mechanism by which NPP1 polymorphisms associated with stroke protection may act.

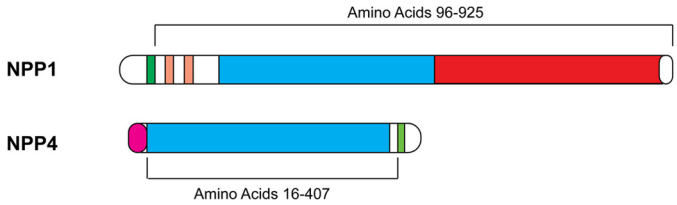

FIGURE 1. **Schematic figure of domain architecture and expressed proteins used in this study.** NPP1 is a type II transmembrane protein, whereas NPP4 is a type I transmembrane protein. The proteins are represented by schematics colored to illustrate the domain architecture as follows. Transmembrane domains are colored *green*; somatomedin B domains are colored *orange*; catalytic domains are colored *cyan*; the nuclease domain is colored *red*, and the signal peptide of NPP4 is colored *magenta*. The expressed NPP1 protein consists of residues 96–925 of the human sequence, comprising the entire extracellular sequence of the protein, containing both somatomedin B domains, the catalytic domain, and the nuclease domain of the protein. The secreted NPP4 protein also consists of the entire extracellular portion of the protein, comprising amino acids 16–407 of the human sequence.

EXPERIMENTAL PROCEDURES

Protein Expression and Purification—Human NPP4 is a type I transmembrane protein, and soluble enzyme was obtained via C-terminal truncation to eliminate the cytoplasmic and transmembrane domains (Fig. 1), as described previously (7). Human NPP1 (NCBI accession NP_006199) was modified to expresses soluble, recombinant protein by replacing its transmembrane region (residues 77–98) with the corresponding subdomain of human NPP2 (NCBI accession NP_001124335, residues 12–30) to allow proteolytic processing of NPP1 on the cell surface as a pre-proprotein, as suggested by Jansen *et al.* (50). The modified NPP1 sequence was cloned into an identical vector as NPP4, and both proteins were expressed using a baculovirus system in insect cells, yielding an accumulation of soluble, recombinant protein secreted into the extracellular fluid, as described previously (7, 51). The C-terminal His tag on these protein constructs allowed for purification via a nickel-nitrilotriacetic acid column. Subsequent tobacco etch virus protease removal of the His tag followed by another nickel-nitrilotriacetic acid column yielded pure protein.

Crystallization, Data Collection and Processing, and Structure Determination—NPP4 was exchanged into 50 mM Tris, pH 8.0, 150 mM NaCl, 0.8 mM $ZnCl_2$, 0.4 mM $CaCl_2$, 0.4 mM $MgCl_2$, and protein concentrations were calculated using A_{280}. The

best diffracting crystals were obtained via hanging drop method by mixing 6 mg/ml (0.14 mM) of NPP4 with well solution (200 mM ammonium citrate dibasic, 17.5–19.5% (w/v) PEG 3350) in a 1:1 ratio and suspending 2 μl drops over 600 μl of the well solution in a sealed chamber. Protein crystals typically appeared within 4–6 days and continued to grow slowly for the next week, reaching final dimensions of up to 500 × 150 × 50 μm. Cryoprotection was achieved by quickly passing the crystals through a series of mixtures consisting of the above well solution with 0.6 mM $ZnCl_2$, 5 mM ligand (if present), and 5% (v/v) increments of glycerol up to a final concentration of 20–25% and then immediately flash-freezing in liquid nitrogen. Apo-crystals of NPP4 were difficult to obtain, hampering efforts to obtain structures of NPP4 with ligands via soaking. Cocrystallization with ATP or a cleavable ATP analog (Sigma M7510) resulted in an AMP product complex, reflecting slow hydrolysis during crystallization. Cocrystallization attempts with a noncleavable ATP analog (Sigma M6517) showed no visible binding.

Synchrotron diffraction data reported herein were collected at APS (Argonne National Laboratory, Advanced Photon Source, NE-CAT beamlines ID-24-C and ID-24-E) and at CHESS (Cornell High Energy Synchrotron Source, beamline A1). HKL2000 was used for indexing and reduction of the NPP4-AMP diffraction data (52). Initial phases were obtained via molecular replacement using PHENIX AutoMR (53) and AutoBuild (54) with a search model consisting of the protein-only portion of the *Xanthomonas axonopodis* NPP (PDB code 2GSU) (55). COOT (56) was employed for model building, and the high quality of initial electron density maps allowed for unambiguous correction of areas of the structure that were originally problematic or out of sequence. PHENIX was used for iterative rounds of maximum likelihood refinement during which ligand, waters, and several glycosylations were built in (57). Apo-NPP4 was solved as above, but using the protein-only portion of the NPP4-AMP complex as the starting point. Unbiased electron density maps in which the local atoms were excluded from map calculations (omit maps) were used to systematically check each entire structure. Atomic positions for all residues 24–402 were determined. Flanking residues at the termini remain disordered. Statistics for diffraction data and the final structures are given in Table 1. The structures of human NPP4-AMP at 1.54 Å resolution (PDB code 4LQY) and apo-NPP4 at 1.50 Å resolution (PDB code 4LR2) have been deposited in the Protein Data Bank.

Molecular Modeling of NPP1-ATP Complex—Mouse NPP1 (PDB code 4B56) was loaded in Molecular Operating Environment (Chemical Computing Group Inc., Montreal, Canada), and the A-chain was deleted and B chain retained with residues Lys-169–Glu-905. Asparagine-linked glycosylation sites were clipped and capped with methyl groups. Waters were deleted and atom types fixed and protonated with Protonate 3D. Zinc ions were restrained with respect to their ligand distance and geometry. The metal charge was modeled at +1. ATP was manually positioned by placing the adenine nucleus between the cleft formed from phenylalanine 239 and tyrosine 322 with the phosphate portion in an extended conformation along the large channel moving up the protein. The protein was tethered at a distance of 4.5 Å from the ligand, and minimization was performed on the entire system using AMBER12 with Extended Huckel Treatment of the ligand (AMBER12:EHT).

Molecular Modeling of NPP4-ATP Complex—NPP4 was modeled in a manner similar to NPP1, including glycosyl stripping and capping and placement of ATP. The corresponding residues in NPP4 for placement of the adenine are phenylalanine 71 and tyrosine 154. Protein protonation, tethering, and minimization were performed in an analogous fashion, using the AMBER12:EHT forcefield treatment.

Enzymology—The steady state enzymatic activity of human NPP1 and NPP4 was determined by either absorbance (Ap3A substrate) or HPLC (ATP substrate) as reported previously (7). The affinities of NMP for NPP4 were estimated from the [NMP] dependence of steady state pNP-TMP cleavage rates as monitored by the absorbance change at 405 nm (51). The [NPP4] was 5 nM, and the [pNP-TMP] was 20 mM. The IC_{50} value (*i.e.* nucleotide concentration exhibiting half-maximal activity) was determined from the best fit of the nucleotide concentration-dependent NPP4 cleavage activity to a rectangular hyperbola. The IC_{50} reflects the weighted average affinity for mixed inhibition (51).

Preparation of Human Platelets and Platelet Aggregometry—Preparation of platelets and platelet aggregometry were performed as described previously (7).

RESULTS

Substrate Discrimination of NPP4 Versus NPP1—To determine the extent of substrate discrimination exhibited by highly homologous NPP family members, we measured the steady state enzymatic rate of human NPP4 and NPP1 for their putative *in vivo* substrates, Ap3A and ATP, respectively (Fig. 2). Human NPP4 shares 40% sequence identity with NPP1 throughout the catalytic domain, and the structure of mouse NPP1 has been recently determined (5, 58) providing the opportunity to identify the structural origins of substrate discrimination at the atomic level. Human and mouse NPP1 are 79% identical, with sequence mapping of the human sequence onto the mouse NPP1 structure showing that all sequence differences are outside the substrate-binding and active sites. Human NPP4 and NPP1 hydrolyze Ap3A with comparable maximum turnover numbers (k_{cat} ~7–8 s^{-1}), although the Michaelis constant of NPP1 is >30 times tighter than that of NPP4. In contrast, the rate at which NPP4 hydrolyzes ATP to AMP and PP_i is negligible compared with hydrolysis by NPP1.

Structural Overview—To understand the molecular basis of NPP4 substrate specificity and to achieve detailed insights regarding its similarities and differences relative to NPP1, we utilized x-ray crystallography to determine the high resolution three-dimensional structures of human NPP4 in both apo- and AMP-bound forms, at 1.50 and 1.54 Å resolution, respectively (Table 1 and Fig. 3*A*). These were then compared with recently determined structures of mouse NPP1 complexes, including mNPP1-AMP at 2.70 Å resolution, to define structural features responsible for the observed substrate specificities of each. The bimetallo catalytic domains of NPP4 and NPP1 contain two bound zinc ions and share a similar overall fold and employ a conserved catalytic mechanism (see below) to hydrolyze at the

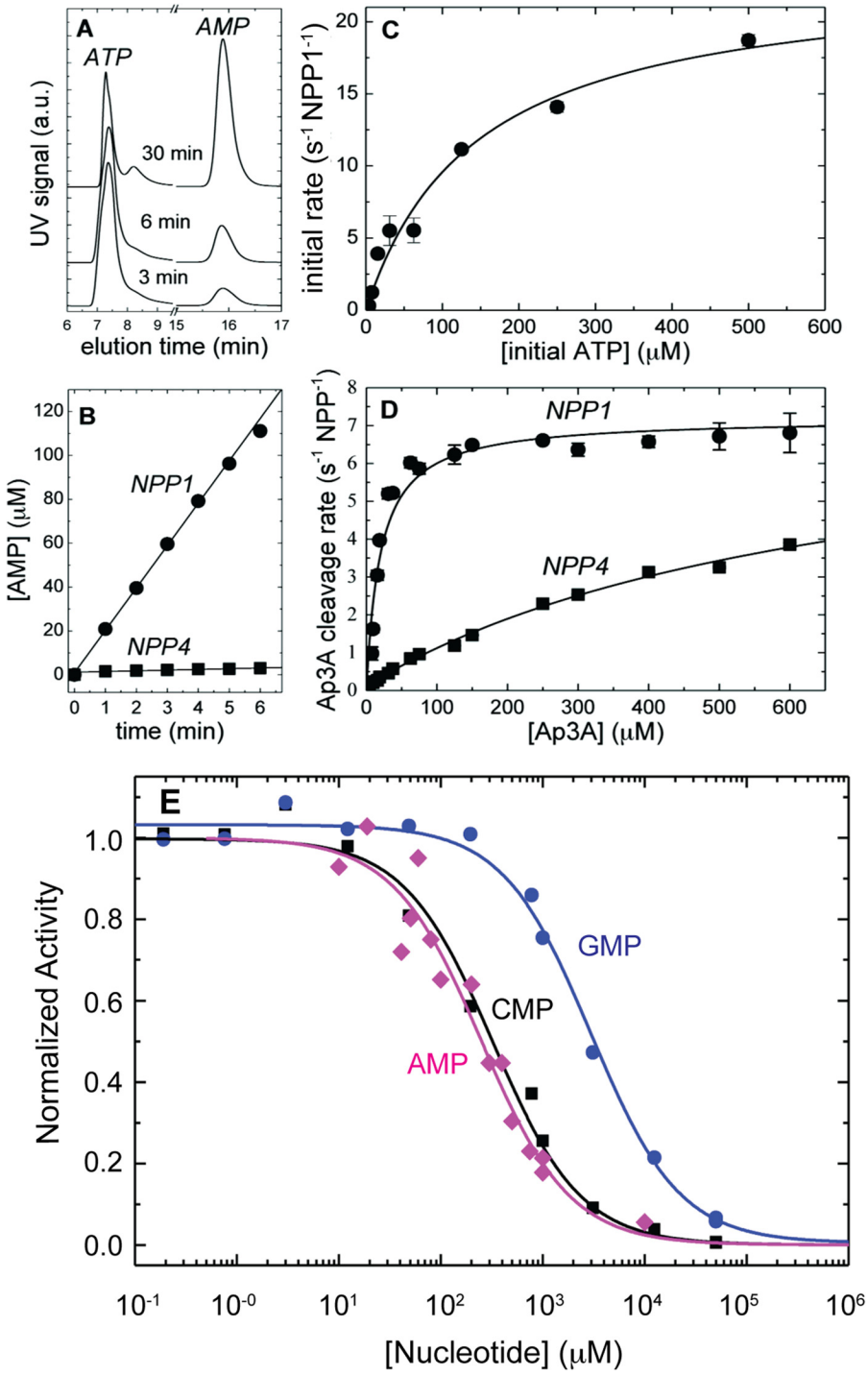

FIGURE 2. **NPP4 and NPP1 substrate specificity.** *A,* HPLC analysis for the reaction samples of 50 nM NPP1 supplemented with 500 μM ATP quenched at (from bottom to top) 3, 6, and 30 min. *a.u.*, absorbance units. *B,* comparison of steady state AMP production from NPP1 (*upper line*) and NPP4 (*lower line*) hydrolysis of 500 μM ATP (initial concentration), analyzed by HPLC. *C,* ATP concentration dependence of the initial steady state velocity of ATP hydrolysis by NPP1 obtained from HPLC analysis. The *smooth line* through the data is the best fit to a hyperbola, resulting in K_m = 144.5 ($\pm$36.0) μM and k_{cat} = 468 ($\pm$48) min^{-1} = 7.8 ($\pm$0.8) s^{-1}. *D,* Ap3A concentration dependence of the NPP1 and NPP4 initial steady state Ap3A substrate cleavage rate obtained from the best linear fits of absorption change of time courses. The smooth lines through the data are the best fit to a hyperbola with K_m = 20 ($\pm$3) μM and k_{cat} = 7.2 ($\pm$0.3) s^{-1} NPP^{-1} for NPP1, whereas with K_m = 685 ($\pm$108) μM and k_{cat} = 8.0 ($\pm$0.1) s^{-1} NPP^{-1} for NPP4. *E,* inhibition of NPP4 cleavage activity by nucleotide monophosphates. The *solid line* through the *data points* represent the best fit to a rectangular hyperbola. Symbols are as follows: AMP, *magenta diamond*; CMP, *black square*; GMP; *blue circle*. The resulting IC50, from strongest to weakest inhibition, is AMP 129 $\pm$ 73 μM, CMP 322 $\pm$ 39 μM, UMP 2.11 $\pm$ 0.37 mM (not shown for clarity), and GMP 2.98 $\pm$ 0.38 mM.

same position on substrates, resulting in a nucleotide monophosphate product. Hydrolysis of Ap3A or ATP by either of these enzymes yields an AMP product molecule. Accordingly, hNPP4-AMP and mNPP1-AMP structures are product complexes. Superposition of the entire catalytic domain of NPP4 with that of NPP1, NPP2, and the bacterial NPP yields r.m.s.d. values of 1.54, 1.43, and 1.43 Å, respectively (Fig. 3*B*). The highest resolution view of a nucleotide-binding NPP prior to this

TABLE 1
Data collection and refinement statistics

	NPP4-AMP	NPP4 apo
Space group	C2	C2
a, *b*, *c*	181.5, 51.1, 52.7 Å	181.5, 51.3, 53.1 Å
α, β, γ	90°, 102.4°, 90°	90°, 102.1°, 90°
Resolution	50 to 1.54 Å	50 to 1.50 Å
Beamline	APS/NE-CAT-C	CHESS/A1
Wavelength	1.0750 Å	0.9779 Å
R_{sym} [a,b]	6.0% (53.6%)	8.4% (54.8%)
$I/\sigma I$ [a,c]	724.9/35.6 (37.0/13.5)	503.2/28.0 (19.0/7.0)
Completeness[a]	99.2% (98.6%)	93.6% (60.2%)
No. of unique reflections	69,525	71,681
Redundancy[a]	4.0 (3.9)	6.8 (5.0)
Monomers/asymmetric unit	1	1
No. of non-hydrogen atoms		
Protein	3069	3069
Ligand (type)[d]	23 (AMP)	13 (FLC)
Metal ions (zinc)	2	2
Glycosylations	56	56
Waters	464	499
Wilson B	17.5	18.1
Average B for:		
Overall	26.4	25.7
Macromolecule	24.3	23.5
Ligand	34.0	29.8
Solvent	40.3	39.6
R_{work}/R_{free} [e,f]	14.0/18.4%	15.4/20.1%
r.m.s.d. bonds	0.009 Å	0.009 Å
r.m.s.d. angles	1.27°	1.20°
Ramachandran plot (%): preferred or allowed/outliers	99.7/0.3	99.5/0.5
Residue range	24–402	24–402
PDB codes	4LQY	4LR2

[a] Values for the highest resolution bin are shown in parentheses.
[b] $R_{sym} = \Sigma_{hkl}\Sigma_i|I_i(hkl) - \langle I(hkl)\rangle|/\Sigma_{hkl}\Sigma_i I_i(hkl)$.
[c] $I/\sigma I$ is the average intensity of reflections in thin resolution bins divided by the average standard deviation (σ) of the same group of reflections.
[d] AMP is ′-adenosine monophosphate. FLC is a citrate anion from the crystallization conditions.
[e] $R_{work} = \Sigma||F_{obs}| - |F_{calc}||/\Sigma|F_{obs}|$.
[f] R_{free} = as for R_{work}, but calculated for 5.0% of the total reflections that were chosen at random and omitted from refinement.

NPP4 structure was a bacterial NPP-AMP complex from *X. axonopodis* at 2.0 Å resolution (55), and the structural features observed in NPP4 that favor nucleotide binding are largely conserved in the bacterial enzyme.

NPP4 is a monomeric enzyme with a binding pocket that remains essentially unchanged in the presence or absence of bound product (Fig. 3*C*). Disulfide bonds link residues 254–287 and 394–401, and three *N*-linked glycosylations were observed at asparagine residues 155, 166, and 386 (data not shown). Because of location, these glycosylations are not likely to significantly impact enzymatic activity. This is the first human NPP structure to be determined and shares an overall common fold with the catalytic domains of all other structurally determined NPPs (Fig. 3*B*).

Substrate Recognition and Active Site Geometry—NPP4 targets phosphodiester substrates with a 5′-nucleotide group on the end, displaying the greatest preference for adenine rings. This specificity for nucleotide-containing substrates is the result of a pre-formed hydrophobic slot on the protein surface, ~6.8 Å wide, consisting of the ring face of Tyr-154 on one side and the tip of Phe-71 on the other side (Fig. 4, *A* and *B*). A nucleotide base bound within experiences favorable π-π stacking interactions with the tyrosine ring and van der Waals interactions with the phenylalanine, sitting about 3.4 Å from each. The back wall of the slot lies just beyond the reach of the nucleotide base, precluding any direct hydrogen bonding interactions with the protein, and only a couple of water-mediated hydrogen bonds were observed between the edge of the AMP ring and NPP4. Although such a slot might be expected to favor purines over pyrimidines by virtue of their greater size, this pattern does not strictly hold. We find that the relative affinities of nucleotide monophosphates for NPP4, as determined by TMP-pNP substrate inhibition, are as follows: AMP > CMP > UMP > GMP (Fig. 2*E*). Corresponding measurements reported for NPP1, another family member with a similar nucleotide slot, reveal the following: AMP > CMP > GMP > UMP (5). Our model building reveals that the guanine ring N2 atom of a similarly bound GMP would experience some steric clash with NPP4 at residues 104 and 105, which slightly overhang the nucleotide slot. Upon inspection of the NPP1-GMP cocrystal structure, we discovered a similar steric clash forcing the guanine ring to rotate slightly.

Immediately adjacent to the hydrophobic slot are two bound zinc ions, hereafter referred to as Zn1 and Zn2 (Fig. 4*B*), held ~4.5 Å apart via interactions with six invariant residues found in all NPPs and alkaline phosphatases (APs). Both zinc ions display tetrahedral coordinate geometry. Zn1 is ligated by Asp-189, His-193, and His-336, with a fourth coordination coming from a phosphate group oxygen atom in the NPP4-AMP complex. Alternatively, in an empty pocket this coordination can be provided by a water molecule. Zn2 is held by Asp-34, Asp-237, and His-238, with a fourth coordination to the Oγ atom of Thr-70, the "catalytic residue" of NPP4. This close association serves to activate Thr-70 for nucleophilic attack on a substrate molecule, as described for APs, presumably by perturbing its pK_a value (59). Thr-70 is located at the N terminus of an α-helix pointing directly at the phosphate-binding site near the semi-exposed Zn1, such that helix-dipole forces complement the positively charged zinc ions in electrostatically drawing the negatively charged phosphodiester group into the active site. The narrow nucleotide slot and the short spacing between the slot and the zinc ions are primarily responsible for substrate selection, sterically favoring a 5′-nucleotide monophosphate group on the end.

By comparison, the other end of the NPP4 binding pocket appears relatively featureless and significantly more solvent-exposed, consistent with the ability of NPP4 to hydrolyze substrates of varying length and chemical character. No crystal structures of any NPP with intact substrate bound have been reported to date; however, our substrate docking simulations indicate that the NPP4 binding pocket runs along the shallow groove on the protein surface.

NPP4-AMP Versus Apo-NPP4—The apo structure of NPP4 is essentially identical to the AMP-bound structure (Fig. 4*C*). Because no changes were observed within the empty hydrophobic slot or at the catalytic residue, the binding site is pre-formed and appears not to undergo induced-fit adjustments upon substrate binding. The apo structure has a citrate anion, from the crystallization conditions, bound at Zn1 in a chelation-like interaction. Asn-91 is the only active site residue that moves notably, pivoting to allow room for the citrate molecule. In the NPP4-AMP complex, Asn-91 donates a hydrogen bond to the

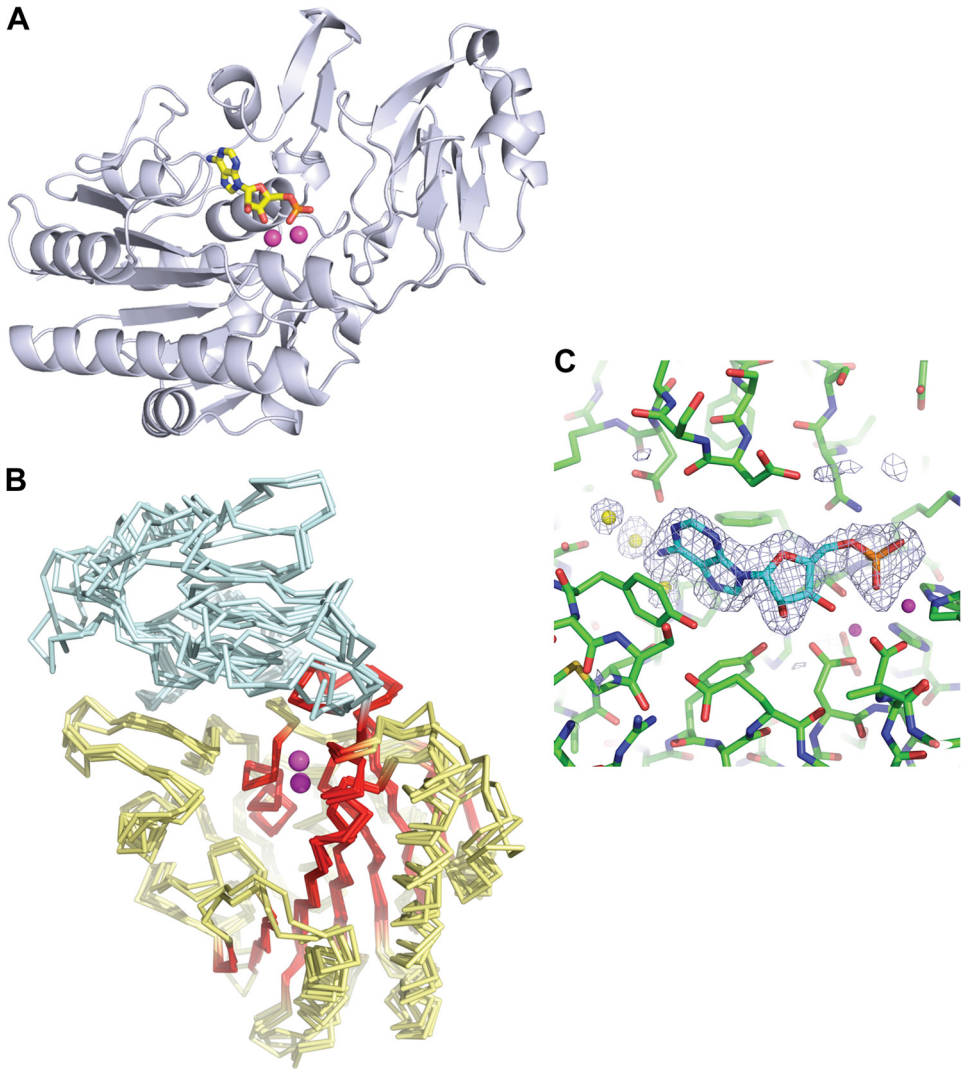

FIGURE 3. **NPP4-AMP structure and comparison with other NPP catalytic domains.** The three-dimensional structure of NPP4 with enzymatic product (AMP) bound was determined to 1.54 Å resolution by x-ray crystallography. *A,* protein is displayed as a *ribbon* with AMP in *stick* form colored by atom type as follows: nitrogen (*blue*), oxygen (*red*), carbon (*yellow*), and phosphorus (*orange*). Active site zinc ions are depicted as *magenta spheres*. *B,* superposition of Cα traces of human NPP4 with other NPP catalytic domains reveals that the greatest degree of structural conservation (shown in *red* with a calculated r.m.s.d. of 0.68 Å for all four molecules as shown) occurs throughout the central β-sheet core and the active site near the zinc ions, including the α-helix on which the catalytic threonine is located and the backbone near the hydrophobic slot. Regions of moderate similarity are *yellow* (average r.m.s.d. of 1.33 Å) and those of the lowest similarity are *cyan* (average r.m.s.d. of 2.51 Å). The ccp4 program Superpose was used to overlay the conserved subdomain (25) (*red-yellow*, r.m.s.d. of 1.17 Å). Despite the high degree of structural conservation near the active site, different NPPs can display widely varying substrate specificities. The four superposed catalytic domains are from human NPP4 (presented here), mouse NPP1 (PDB code 4B56), mouse NPP2 (PDB code 3NKN), and a bacterial NPP (PDB code 2GSU). To accommodate a lipid substrate, NPP2 lacks a region found in all other NPP catalytic domains, and therefore an 8-residue linker (residues 272–279) within mouse NPP2 was omitted in this comparison figure. Superposition of the entire catalytic domain of NPP4 with that of NPP1, NPP2, and the bacterial NPP yields r.m.s.d. values of 1.54, 1.43, and 1.43 Å, respectively. *C,* NPP4 product complex with AMP. Omit m$F_o - \Delta F_c$ difference density is shown for each, contoured at 3σ. Ligands and water molecules within the binding pocket were not included in the electron density map calculations. PyMOL was used to generate all molecular images (Molecular Graphics System, Version 1.2r3pre, Schrödinger, LLC).

phosphate group bound near Zn1. The ability of Asn-91 to pivot may allow it to maintain a hydrogen bonding interaction with the phosphate oxygen through the catalytic intermediates of the reaction or allow flexibility to facilitate the entry or exit of a ligand.

NPP4-AMP Versus NPP1-AMP—The overall similarity of how AMP binds within the slot region of NPP4 and NPP1 is shown in Fig. 4*D*. NPP1 contains conserved residues corresponding to Tyr-154 and Phe-71 of NPP4, and therefore it also targets substrates with a 5′-nucleotide end. The phosphate group of AMP binds near Zn1 in both enzymes. Whether the small differences observed in AMP position are real or simply reflect the significantly lower resolution of the NPP1-AMP structure (2.70 Å *versus* 1.54 Å for NPP4-AMP) is unknown.

Catalytic Mechanism—NPPs are members of the AP superfamily and share many of the key structural features, residues, and architecture at the center of the active site where the catalysis occurs. Gijsbers *et al.* (60) proposed a general reaction mechanism for NPPs based on active site homology to APs. Fig. 5 depicts that mechanism as it applies to NPP4 hydrolysis of Ap3A, along with the corresponding crystal structures indicated. In NPP4, the relative spacing between the pre-formed hydrophobic slot and the two bound zinc ions dictates that it is the α-phosphate group of the substrate that is positioned adja-

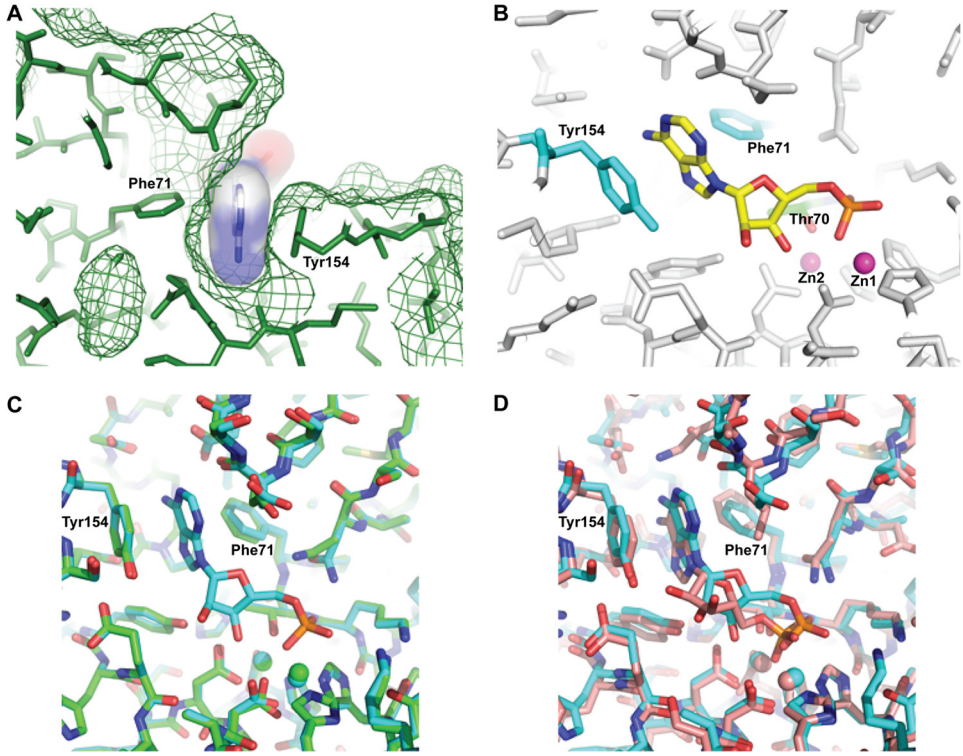

FIGURE 4. **Detail of base recognition of substrate at the NPP4 catalytic site.** *A,* active site of NPP4 contains a pre-formed hydrophobic slot that results in its specificity for 5′-nucleotide-containing substrates. In the NPP4-AMP complex, the adenine ring stacks with Tyr-154 on one wall of the pocket while receiving favorable van der Waals interactions from the tip of Phe-71 along the opposite wall. To display the fit, the molecular surface of NPP4 (*green mesh*) and the van der Waals surface of AMP (*semi-transparent*) are shown. *B,* position of AMP in the active site with key residues and bound-metal ions highlighted. The two bound zinc ions (*magenta spheres*) play different roles, with Zn2 serving to activate Thr-70 (*green*) for nucleophilic attack on the substrate, whereas Zn1 electrostatically draws a phosphate group of the substrate into close proximity. Tyr-154 and Phe-71 of the nucleotide slot are shown in *cyan*. *C,* superposition of the NPP4-AMP complex (*blue*) with apo-NPP4 (*green*) to illustrate that there is very little change when product is bound. A citrate anion bound at Zn1 of the apo structure has been omitted for visual clarity. *D,* superposition of NPP4-AMP (*blue*) and NPP1-AMP (*salmon*) complexes to illustrate the similar geometry within this half of their active sites, with both possessing a slot for nucleotide binding.

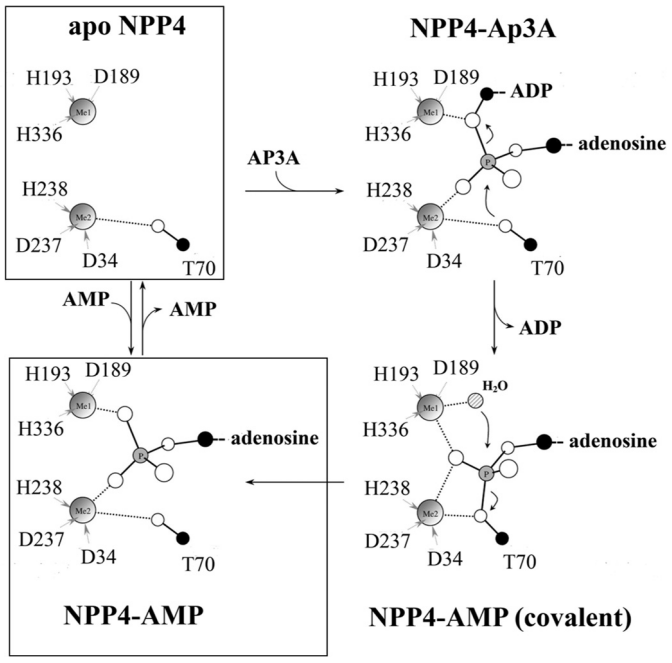

FIGURE 5. **Proposed enzymatic mechanism of Ap3A hydrolysis by NPP4.** Proposed reaction mechanism for NPP4 hydrolysis of Ap3A is based on active site homology to APs as originally proposed by Gijsbers *et al.* (60). *Boxes* have been placed around the steps in the mechanism for which crystal structures have been obtained. Oxygen atoms are depicted as *white balls*.

cent to the Zn1 and Thr-70, whose Oγ atom is perpetually activated for nucleophilic attack by its close proximity to Zn2. Upon Ap3A binding, the α-phosphate is attacked by Thr-70, causing the ester bond on the opposite side to break, releasing ADP. A water molecule immediately enters the vacant space next to Zn1, becomes activated, and attacks the α-phosphate from the opposite direction, causing the transient covalent NPP4-AMP bond to break, releasing AMP and restoring NPP4 to its original state. The release of the two product molecules is sequential, with the nucleotide monophosphate leaving last. As such, NPP4-AMP and NPP1-AMP are product complexes.

Molecular Determinants of Substrate Specificity of NPP4 and NPP1—NPP1 readily cleaves ATP into AMP and PP_i, whereas NPP4 does so only exceedingly slowly. Because both enzymes target nucleotide-containing substrates with a preference for adenine rings, and bind AMP in a similar fashion (Fig. 4*D*), the key to this deviation must lie elsewhere within the binding pocket. Because NPP1 efficiently hydrolyzes ATP into AMP and PP_i, ATP likely binds NPP1 in the same orientation as is observed for AMP. We therefore modeled ATP into the NPP1 active site by adding two phosphate groups to the NPP1-AMP cocrystal coordinates (PDB code 4B56) (Fig. 6, *A*, *C,* and *E*) and then subjected the complex to energy minimization as described. Superposition of the binding sites of NPP1 with NPP4 reveals good overlap between most side chains within 4.5 Å of this ATP substrate, but with notable differences occurring

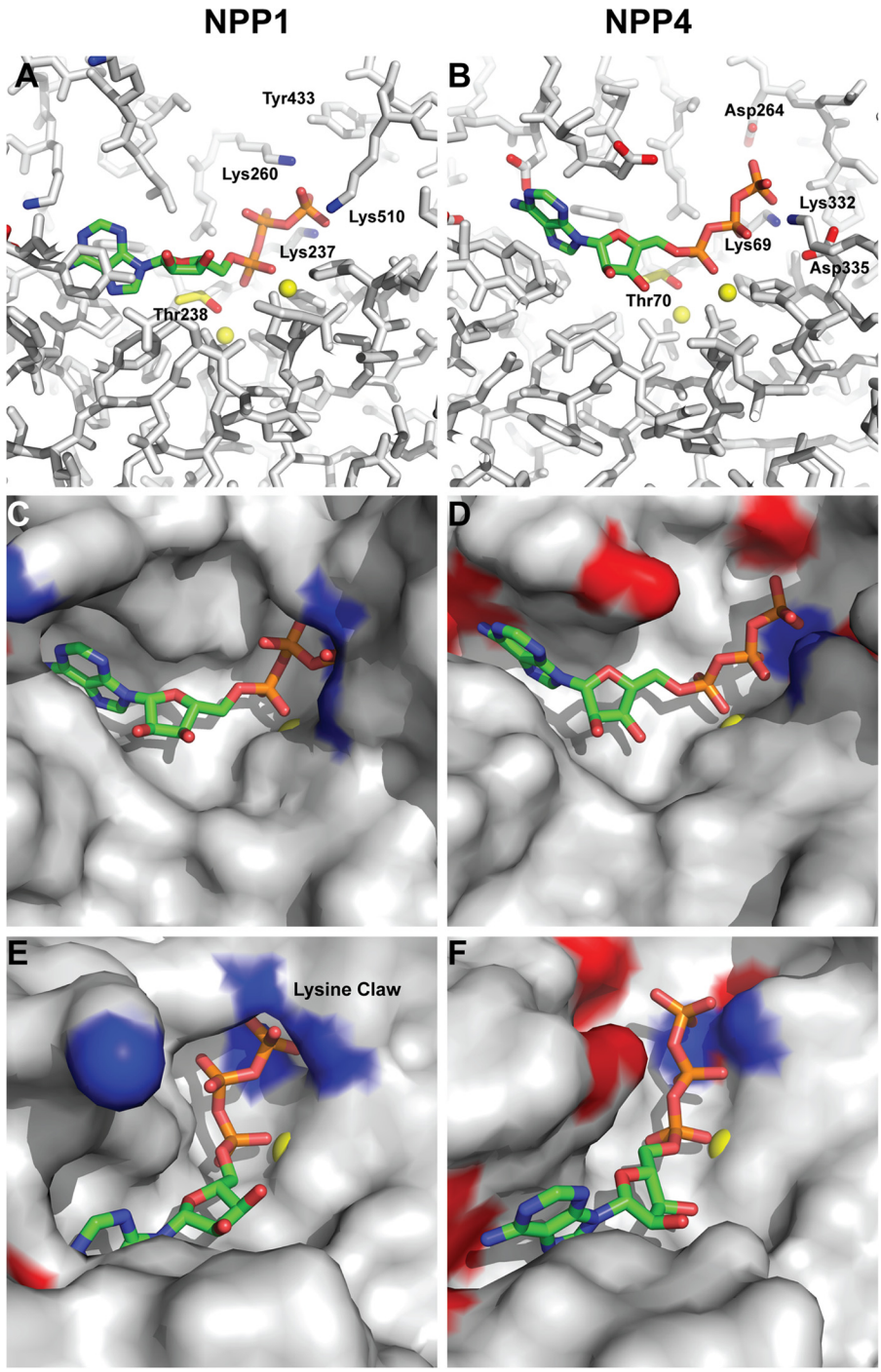

FIGURE 6. **Modeling the molecular basis of substrate discrimination of NPP1 and NPP4.** Energy-minimized models' of ATP bound in an AMP-like orientation are shown for NPP1 (*left column*) and NPP4 (*right column*), based on the AMP cocrystal structures for each enzyme. In NPP1, the γ-phosphate of ATP is simultaneously stabilized by three lysine residues, two of which line the upper edge of the pocket and become ordered only when substrate is present due to electrostatics. As a result of this tri-partite lysine claw, the γ-phosphate of bound ATP is favorably charge-stabilized and largely shielded from solvent by an induced-fit lid comprised of the long hydrophobic side chains of these two lysines along with an adjacent tyrosine ring. In contrast, NPP4 offers a significantly less favorable γ-phosphate environment for a similarly bound ATP, with less charge stabilization, a more open architecture with no lid mechanism, and two nearby aspartate residues for charge repulsion. As a result, ATP is not likely to bind in this orientation to NPP4 very often. *A* and *B, stick figures* of ATP bound, as modeled from AMP cocrystal structures. *C* and *D,* same, but as a molecular surface with tips of nearby charged side chains colored *blue* (positive) and *red* (negative). *E* and *F,* rotated about 90°. Sequence alignments show that human NPP1 retains all of the features derived from the mouse NPP1 structure.

near the terminal γ-phosphate. In NPP1, donation of Phe-516 (mouse numbering) to the protein core creates more space for the γ-phosphate of ATP, which appears to be charge-stabilized by three lysine residues (Lys-237, Lys-260, and Lys-510), which we refer to as a lysine claw. Two of these lysines (Lys-260 and Lys-510) line the upper edge of the binding pocket and remain disordered in the absence of a γ-phosphate, as is observed in the NPP1-AMP structure (5, 58). Our simulation shows that as new substrate enters the NPP1-binding site, these lysines should be electrostatically drawn to the γ-phosphate and become ordered

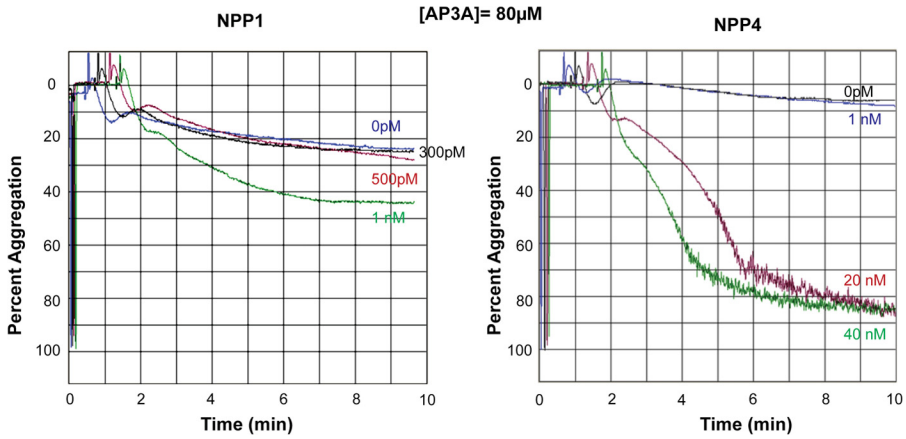

FIGURE 7. **NPP1 effect on platelet aggregation.** Light transmission aggregometry was used to assess platelet aggregation in response to increasing concentrations of NPP1 and NPP4 and 80 μM Ap3A in platelet-rich plasma. Data are shown graphically as percent of light transmittance (*y* axis) over time (*x* axis). *Left panel,* in the absence of NPP1, 80 μM Ap3A elicits only a primary wave of aggregation followed by rapid disaggregation (*blue tracing*), and this pattern is similarly observed with the addition of NPP1 in concentrations of 300 and 500 pM (*black* and *red tracings*, respectively). In contrast, 1 nM NPP1 in the presence of 80 μM Ap3A stimulates a measurable secondary wave of aggregation (*green tracing*). *Right panel,* NPP4 exhibits primary aggregation in the presence of either Ap3A alone or Ap3A containing 1 nM NPP4. In the presence of 20 nM NPP4 and higher, there is marked secondary platelet aggregation. The findings support the notion that either protein may directly stimulate platelet aggregation at low nanomolar concentrations in the presence of physiologic concentrations of Ap3A.

in the process. The γ-phosphate of bound ATP appears to lie under an induced-fit lid comprised of Tyr-433, Lys-260, and Lys-510, where it should be charge-stabilized by three lysines (Fig. 6*A*). Upon PP_i product release, Lys-260 and Lys-510 should again become disordered until new substrate is drawn to the site.

In a likewise manner, ATP was modeled into the NPP4 active site by adding two phosphates onto the NPP4-AMP structure, after which the complex was energy-minimized. In contrast to NPP1, the region of NPP4 near the γ-phosphate is much more open and solvent-exposed, contains additional negatively charged residues and fewer positively charged ones, and has no ability to form a lysine claw or lid (Fig. 6, *B*, *D,* and *F*). The γ-phosphate of ATP bound in this orientation would sit next to the negatively charged Asp-335, which corresponds to Phe-516 of NPP1, but now points directly into the binding pocket. Asp-264 (corresponding to Val-432, mouse NPP1) is also nearby. Overall, the local electrostatic environment of this region of the NPP4 binding pocket is significantly less favorable than in NPP1.

The ability to charge-stabilize at this position may be more pronounced with ATP than with other substrates, such as Ap3A, because a terminal phosphate group (phosphomonoester) intrinsically carries more negative charge than a nonterminal phosphate group (phosphodiester). As such, the terminal γ-phosphate of ATP carries more negative charge than the corresponding in-line γ-phosphate of Ap3A. The highly effective charge stabilization of NPP1 at this position is likely key to its ability to readily hydrolyze ATP, whereas the less favorable local environment found at this same position in NPP4 is detrimental, and hydrolysis occurs only very slowly.

NPP1 and Platelet Aggregation—The hydrolysis of Ap3A by NPP1 raises the question of whether NPP1 may play a role in platelet aggregation under physiologic conditions. Given that the enzyme is active against Ap3A substrate, the relative abundance of NPP1 within the vascular space will determine the role of NPP1 in coagulation. An important observation in this regard is that NPP1 is reported to be present on brain capillary endothelium but not on capillaries elsewhere (61). In addition, NPP1 is principally present on the membrane surfaces of plasma cells, osteoblasts, chondrocytes, and matrix vesicles shed from osteoblasts and chondrocytes. NPP1 is also reported to be present as a soluble protein within the vasculature at very low concentrations between 10 and 30 ng/ml (or 100–300 pM) (62). To determine the concentration of NPP1 capable of inducing platelet aggregation, we titrated increasing concentrations of NPP1 into platelet-rich plasma with physiologic levels of Ap3A. Addition of NPP1 to 80 μM Ap3A results in no platelet aggregation until the concentrations of NPP1 reach 1 nM (Fig. 7). Although this concentration is ~3-fold greater than the highest reported plasma concentrations of NPP1, this concentration is below the threshold required for NPP4 to trigger platelet aggregation (Fig. 7) and is well within the concentration range of membrane-bound endothelial proteins. We therefore surmise that plasma concentrations of NPP1 are unlikely to induce primary platelet-mediated hemostasis *in vivo* but that epithelium-bound NPP1 at anatomic locations, where local concentrations exceed 1 nM, are likely to induce significant platelet aggregation and thrombus formation.

DISCUSSION

Our high resolution structural determination of human NPP4 allowed for detailed comparative structure-function studies with NPP1. These membrane-bound cell surface enzymes are involved in the metabolism of extracellular purinergic signals as well as nucleotide re-uptake. Both ectoenzymes possess a narrow hydrophobic slot adjacent to two bound zinc ions, which accounts for the targeting of nucleotide-containing substrates, where the nucleotide base binds within the slot and hydrolysis yields the nucleotide monophosphate as one of the products. Adenine is the most preferred base type for both enzymes, and cocrystal structures of each with a product AMP molecule bound highlight their functional similarity in that region of the binding site. We demonstrate that

both enzymes are able to hydrolyze Ap3A but exhibit surprisingly different responses to ATP.

For all of their similarities, NPP4 and NPP1 differ drastically in their response to ATP. NPP1 readily hydrolyzes ATP to AMP and PP_i, the latter of which is a potent inhibitor of extra-osseous mineralization, and mutants of NPP1 have been linked to a variety of diseases involving bone or soft tissue calcification outlined earlier. To yield the observed products, ATP should bind NPP1 in the same orientation seen in the NPP1-AMP cocrystal structure. In stark contrast, NPP4 cleaves ATP only exceedingly slowly, even though it binds AMP in a manner very similar to NPP1. Superposition of the two enzymes reveals key structural differences in the area of the terminal phosphate of ATP, if bound like AMP. Our energy-minimized simulations of ATP complexes reveal that NPP1 provides a favorable environment for the γ-phosphate of ATP via the presence of a tripartite lysine claw that provides induced-fit charge stabilization. In the absence of substrate, two lysines lining the upper ridge of the binding pocket (Lys-260 and Lys-510, mouse numbering) are mobile, as is demonstrated in the NPP1-AMP product complex (PDB code 4GTW) where they are disordered or in the NPP1-vanadate complex (PDB code 4B56) where they exhibit high *B*-factors and extend into the solvent. Upon ATP substrate binding, the highly negative γ-phosphate should electrostatically attract these lysines, which along with the stationary Lys-237 on the floor of the binding pocket should serve to effectively envelop the terminal phosphate in positive charge. This may also promote the hydrolysis via product stabilization, because PP_i is even more negatively charged. The role these lysine residues play in NPP1 hydrolysis of ATP had not been previously appreciated and came to light during our detailed structural comparisons with NPP4.

Superposition of the corresponding region of NPP4 shows it to be notably less favorable for a similarly bound ATP, with a local architecture that is more open, contains fewer positively charged residues, and introduces negatively charged residues such as Asp-335, which likely projects into the active site in close proximity to the γ-phosphate of ATP. Cocrystallization attempts with a noncleavable ATP analog revealed no visible binding, consistent with our observation that NPP4 provides an unfavorable environment in the region of the γ-phosphate. Similarly, cocrystallization attempts with ATP or a cleavable ATP analog yield an AMP complex over the several days it takes for crystals to grow, indicating that although ATP binding is weak, it occasionally comes into close enough proximity to be hydrolyzed. The AMP product molecule is able to bind under identical conditions, reflecting a stronger affinity. Product inhibition is likely an intrinsic feature of NPP reactions because the phosphate group next to Zn1 gets converted, by definition, from a phosphodiester to a terminal phosphate that carries more negative charge. Our data indicate that NPP4 is unlikely to hydrolyze ATP effectively *in vivo*, supporting the view that NPP1 is the primary extracellular enzyme metabolizing purinergic signals regulating bone remodeling and extracellular calcification.

In contrast, both NPP4 and NPP1 hydrolyze Ap3A into AMP and ADP, with the Michaelis constant of NPP1 for Ap3A some 30-fold tighter than that of NPP4. This higher affinity is reflected in the lower concentrations of NPP1 required to trigger platelet aggregation in identical concentrations of Ap3A (Fig. 7). High concentrations of Ap3A stored in the dense granules of circulating platelets are released upon platelet activation. We recently proposed that vascular bound NPPs could contribute to cerebral platelet aggregation by identifying NPP4 on brain vascular endothelium capable of inducing platelet aggregation via the hydrolysis of physiologic concentrations of Ap3A (7). Ap3A has a significantly longer life span in whole blood than ADP and has long been hypothesized to aid stable thrombus formation by serving as a chemically masked source of ADP.

The ability of NPP1 to readily hydrolyze Ap3A to ADP raises the question of whether NPP1 may play a role in hemostasis. In this study, we demonstrate that NPP1 is capable of Ap3A hydrolysis at low nanomolar concentrations, and either NPP1 or NPP4 at these concentrations promotes irreversible platelet aggregation in human platelet-rich plasma *in vitro*. Our work implies that either enzyme may contribute significantly to platelet aggregation *in vivo* if present at low nanomolar concentrations in a pro-thrombotic environment.

Recently, polymorphisms in NPP1 have been identified that confer stroke protection in pediatric patients with sickle cell anemia (49). Stroke is a devastating complication in pediatric sickle cell patients, with 5–10% of patients experiencing a clinically overt thrombotic stroke during childhood. An unbiased whole genome search for genetic modifiers of stroke risk identified the K173Q mutation in NPP1 to be significantly associated with decreased risk for stroke. Flanagan *et al.* (49) hypothesize that the protective effects of the NPP1 polymorphism represent a gain of function mutation that increases serum PP_i concentrations, thereby inhibiting stroke via an undefined mechanism. This opinion appears posited in part by equating the K173Q mutation with the K121Q mutation associated with type 2 insulin-dependent diabetes mellitus (IDDM-2), which increases serum concentrations of NPP1 from 24 to 28 ng/ml (63, 64). Our studies suggest an alternative hypothesis, *i.e.* that polymorphisms in NPP1 protective against stroke represent a loss of function mutation that decreases Ap3A hydrolysis in the thrombotic microenvironment. If NPP1 is indeed present on brain capillaries as reported (61), decreased NPP1 activity would result in decreased ADP concentrations in the cerebral capillary bed, thus providing a direct mechanism to account for decreased platelet aggregation and thrombus formation.

The K173Q mutation in human NPP1 is not in the catalytic domain but rather is found in the somatomedin B-2 domain near the membrane spanning region (Fig. 1). Loss of function mutations within the NPP1 catalytic domain are not compatible with human survival beyond the neonatal period, consistent with their absence in the population screened for stroke protection. Although NPP1 K173Q mutations may increase NPP1 serum concentrations similarly to K121Q mutations observed in IDDM-2, we do not find arguments for the NPP1 gain of function based on these serum increases to be compelling, especially when viewed in light of our kinetic and aggregometry data. NPP1 serum concentrations in the K121Q polymorphism (28 pM) are well below those required for NPP1-induced activation of platelet aggregation *in vitro*, and the Michaelis con-

stant of NPP1 for both ATP and Ap3A is nearly 10^6 higher than the 40 pM increase induced by the K121Q polymorphism, suggesting that the increase is unlikely to impact either systemic PP_i or ADP concentrations. A possible mechanism for changes attributed to the NPP1 K173Q polymorphism could be increased ectodomain shedding of NPP1 from vascular endothelium, which would account for both increases in serum levels and the loss of NPP1 activity on vascular endothelium now denuded of the protein. In summation, although the means by which a K173Q mutation impairs NPP1 catalytic activity remain obscure, our findings support the notion that NPP1 polymorphisms protective against stroke are more likely to represent loss of function mutations that decrease Ap3A hydrolysis on the endothelial surface of cerebral capillary beds than gain of function mutations that increase PP_i concentrations.

In this study, we present the molecular determinants of substrate specificity for NPP4 and NPP1 in extracellular nucleotide metabolism, and we demonstrate that NPP1 has significant Ap3A hydrolytic activity capable of inducing platelet aggregation at low nanomolar concentrations. Our findings provide a molecular foundation for understanding the enzymatic and physiologic roles of the enzymes and their contribution to disorders of ectopic bone mineralization and thrombosis. These studies may be helpful to those seeking to design small molecule modulators of purigenic signals involved in thrombotic disorders and bone mineralization.

Acknowledgments—We are indebted to Joe Madri for many useful discussions and guidance and to Dr. Jon Morrow for enthusiastic support and encouragement throughout the course of this investigation.

REFERENCES

1. Offermanns, S. (2006) Activation of platelet function through G-protein-coupled receptors. *Circ. Res.* **99,** 1293–1304
2. Terkeltaub, R. (2006) Physiologic and pathologic functions of the NPP nucleotide pyrophosphatase/phosphodiesterase family focusing on NPP1 in calcification. *Purinergic Signal.* **2,** 371–377
3. Omatsu-Kanbe, M., Isono, T., and Matsuura, H. (2002) Multiple P2 receptors contribute to a transient increase in intracellular Ca^{2+} concentration in ATP-stimulated rat brown adipocytes. *Exp. Physiol.* **87,** 643–652
4. Schödel, J., Weise, I., Klinger, R., and Schmidt, M. (2004) Stimulation of lipogenesis in rat adipocytes by ATP, a ligand for P2-receptors. *Biochem. Biophys. Res. Commun.* **321,** 767–773
5. Kato, K., Nishimasu, H., Okudaira, S., Mihara, E., Ishitani, R., Takagi, J., Aoki, J., and Nureki, O. (2012) Crystal structure of Enpp1, an extracellular glycoprotein involved in bone mineralization and insulin signaling. *Proc. Natl. Acad. Sci. U.S.A.* **109,** 16876–16881
6. Vollmayer, P., Clair, T., Goding, J. W., Sano, K., Servos, J., and Zimmermann, H. (2003) Hydrolysis of diadenosine polyphosphates by nucleotide pyrophosphatases/phosphodiesterases. *Eur. J. Biochem.* **270,** 2971–2978
7. Albright, R. A., Chang, W. C., Robert, D., Ornstein, D. L., Cao, W., Liu, L., Redick, M. E., Young, J. I., De La Cruz, E. M., and Braddock, D. T. (2012) NPP4 is a procoagulant enzyme on the surface of vascular endothelium. *Blood* **120,** 4432–4440
8. Tokumura, A., Majima, E., Kariya, Y., Tominaga, K., Kogure, K., Yasuda, K., and Fukuzawa, K. (2002) Identification of human plasma lysophospholipase D, a lysophosphatidic acid-producing enzyme, as autotaxin, a multifunctional phosphodiesterase. *J. Biol. Chem.* **277,** 39436–39442
9. Umezu-Goto, M., Kishi, Y., Taira, A., Hama, K., Dohmae, N., Takio, K., Yamori, T., Mills, G. B., Inoue, K., Aoki, J., and Arai, H. (2002) Autotaxin has lysophospholipase D activity leading to tumor cell growth and motility by lysophosphatidic acid production. *J. Cell Biol.* **158,** 227–233
10. Saunders, L. P., Cao, W., Chang, W. C., Albright, R. A., Braddock, D. T., and De La Cruz, E. M. (2011) Kinetic analysis of autotaxin reveals substrate-specific catalytic pathways and a mechanism for lysophosphatidic acid distribution. *J. Biol. Chem.* **286,** 30130–30141
11. Sakagami, H., Aoki, J., Natori, Y., Nishikawa, K., Kakehi, Y., Natori, Y., and Arai, H. (2005) Biochemical and molecular characterization of a novel choline-specific glycerophosphodiester phosphodiesterase belonging to the nucleotide pyrophosphatase/phosphodiesterase family. *J. Biol. Chem.* **280,** 23084–23093
12. Duan, R. D., Bergman, T., Xu, N., Wu, J., Cheng, Y., Duan, J., Nelander, S., Palmberg, C., and Nilsson, A. (2003) Identification of human intestinal alkaline sphingomyelinase as a novel ecto-enzyme related to the nucleotide phosphodiesterase family. *J. Biol. Chem.* **278,** 38528–38536
13. Liu, S., Umezu-Goto, M., Murph, M., Lu, Y., Liu, W., Zhang, F., Yu, S., Stephens, L. C., Cui, X., Murrow, G., Coombes, K., Muller, W., Hung, M. C., Perou, C. M., Lee, A. V., Fang, X., and Mills, G. B. (2009) Expression of autotaxin and lysophosphatidic acid receptors increases mammary tumorigenesis, invasion, and metastases. *Cancer Cell* **15,** 539–550
14. Boucharaba, A., Serre, C. M., Guglielmi, J., Bordet, J. C., Clézardin, P., and Peyruchaud, O. (2006) The type 1 lysophosphatidic acid receptor is a target for therapy in bone metastases. *Proc. Natl. Acad. Sci. U.S.A.* **103,** 9643–9648
15. Raj, G. V., Sekula, J. A., Guo, R., Madden, J. F., and Daaka, Y. (2004) Lysophosphatidic acid promotes survival of androgen-insensitive prostate cancer PC3 cells via activation of NF-κB. *Prostate* **61,** 105–113
16. Kishi, Y., Okudaira, S., Tanaka, M., Hama, K., Shida, D., Kitayama, J., Yamori, T., Aoki, J., Fujimaki, T., and Arai, H. (2006) Autotaxin is overexpressed in glioblastoma multiforme and contributes to cell motility of glioblastoma by converting lysophosphatidylcholine to lysophosphatidic acid. *J. Biol. Chem.* **281,** 17492–17500
17. Sevastou, I., Kaffe, E., Mouratis, M. A., and Aidinis, V. (2013) Lysoglycerophospholipids in chronic inflammatory disorders: The PLA(2)/LPC and ATX/LPA axes. *Biochim. Biophys. Acta* **1831,** 42–60
18. Tager, A. M., LaCamera, P., Shea, B. S., Campanella, G. S., Selman, M., Zhao, Z., Polosukhin, V., Wain, J., Karimi-Shah, B. A., Kim, N. D., Hart, W. K., Pardo, A., Blackwell, T. S., Xu, Y., Chun, J., and Luster, A. D. (2008) The lysophosphatidic acid receptor LPA1 links pulmonary fibrosis to lung injury by mediating fibroblast recruitment and vascular leak. *Nat. Med.* **14,** 45–54
19. Tanaka, M., Okudaira, S., Kishi, Y., Ohkawa, R., Iseki, S., Ota, M., Noji, S., Yatomi, Y., Aoki, J., and Arai, H. (2006) Autotaxin stabilizes blood vessels and is required for embryonic vasculature by producing lysophosphatidic acid. *J. Biol. Chem.* **281,** 25822–25830
20. van Meeteren, L. A., Ruurs, P., Stortelers, C., Bouwman, P., van Rooijen, M. A., Pradère, J. P., Pettit, T. R., Wakelam, M. J., Saulnier-Blache, J. S., Mummery, C. L., Moolenaar, W. H., and Jonkers, J. (2006) Autotaxin, a secreted lysophospholipase D, is essential for blood vessel formation during development. *Mol. Cell. Biol.* **26,** 5015–5022
21. Bertrand, J., Nitschke, Y., Fuerst, M., Hermann, S., Schäfers, M., Sherwood, J., Nalesso, G., Ruether, W., Rutsch, F., Dell'Accio, F., and Pap, T. (2012) Decreased levels of nucleotide pyrophosphatase phosphodiesterase 1 are associated with cartilage calcification in osteoarthritis and trigger osteoarthritic changes in mice. *Ann. Rheum. Dis.* **71,** 1249–1253
22. Rutsch, F., Ruf, N., Vaingankar, S., Toliat, M. R., Suk, A., Höhne, W., Schauer, G., Lehmann, M., Roscioli, T., Schnabel, D., Epplen, J. T., Knisely, A., Superti-Furga, A., McGill, J., Filippone, M., Sinaiko, A. R., Vallance, H., Hinrichs, B., Smith, W., Ferre, M., Terkeltaub, R., and Nürnberg, P. (2003) Mutations in ENPP1 are associated with "idiopathic" infantile arterial calcification. *Nat. Genet.* **34,** 379–381
23. Mackenzie, N. C., Zhu, D., Milne, E. M., van 't Hof, R., Martin, A., Darryl Quarles, L., Quarles, D. L., Millán, J. L., Farquharson, C., and MacRae, V. E. (2012) Altered bone development and an increase in FGF-23 expression in Enpp1(−/−) mice. *PLoS One* **7,** e32177
24. Stefan, C., Jansen, S., and Bollen, M. (2005) NPP-type ectophosphodiesterases: unity in diversity. *Trends Biochem. Sci.* **30,** 542–550
25. Collaborative Computational Project No. 4 (1994) The CCP4 suite: programs for protein crystallography. *Acta Crystallogr. D Biol. Crystallogr.* **50,** 760–763

26. Gachet, C. (2012) P2Y(12) receptors in platelets and other hematopoietic and non-hematopoietic cells. *Purinergic Signal.* **8,** 609–619
27. Enjyoji, K., Sévigny, J., Lin, Y., Frenette, P. S., Christie, P. D., Esch, J. S., 2nd, Imai, M., Edelberg, J. M., Rayburn, H., Lech, M., Beeler, D. L., Csizmadia, E., Wagner, D. D., Robson, S. C., and Rosenberg, R. D. (1999) Targeted disruption of cd39/ATP diphosphohydrolase results in disordered hemostasis and thromboregulation. *Nat. Med.* **5,** 1010–1017
28. Kaczmarek, E., Koziak, K., Sévigny, J., Siegel, J. B., Anrather, J., Beaudoin, A. R., Bach, F. H., and Robson, S. C. (1996) Identification and characterization of CD39/vascular ATP diphosphohydrolase. *J. Biol. Chem.* **271,** 33116–33122
29. Marcus, A. J., Broekman, M. J., Drosopoulos, J. H., Islam, N., Alyonycheva, T. N., Safier, L. B., Hajjar, K. A., Posnett, D. N., Schoenborn, M. A., Schooley, K. A., Gayle, R. B., and Maliszewski, C. R. (1997) The endothelial cell ecto-ADPase responsible for inhibition of platelet function is CD39. *J. Clin. Invest.* **99,** 1351–1360
30. Knowles, A. F. (2011) The GDA1_CD39 superfamily: NTPDases with diverse functions. *Purinergic Signal.* **7,** 21–45
31. Pearson, J. D., and Gordon, J. L. (1985) Nucleotide metabolism by endothelium. *Annu. Rev. Physiol.* **47,** 617–627
32. Birk, A. V., Bubman, D., Broekman, M. J., Robertson, H. D., Drosopoulos, J. H., Marcus, A. J., and Szeto, H. (2002) Role of a novel soluble nucleotide phosphohydrolase from sheep plasma in inhibition of platelet reactivity: Hemostasis, thrombosis, and vascular biology. *J. Lab. Clin. Med.* **139,** 116–124
33. Yegutkin, G. G. (2008) Nucleotide- and nucleoside-converting ectoenzymes: Important modulators of purinergic signalling cascade. *Biochim. Biophys. Acta* **1783,** 673–694
34. Zimmermann, H. (1992) 5′-Nucleotidase: molecular structure and functional aspects. *Biochem. J.* **285**, 345–365
35. Koszalka, P., Ozüyaman, B., Huo, Y., Zernecke, A., Flögel, U., Braun, N., Buchheiser, A., Decking, U. K., Smith, M. L., Sévigny, J., Gear, A., Weber, A. A., Molojavyi, A., Ding, Z., Weber, C., Ley, K., Zimmermann, H., Gödecke, A., and Schrader, J. (2004) Targeted disruption of cd73/ecto-5′-nucleotidase alters thromboregulation and augments vascular inflammatory response. *Circ. Res.* **95,** 814–821
36. Lüthje, J., and Ogilvie, A. (1983) The presence of diadenosine 5′,5‴-P1,P3-triphosphate (Ap3A) in human platelets. *Biochem. Biophys. Res. Commun.* **115,** 253–260
37. Lüthje, J., Miller, D., and Ogilvie, A. (1987) Unproportionally high concentrations of diadenosine triphosphate (Ap3A) and diadenosine tetraphosphate (Ap4A) in heavy platelets. Consequences for in vitro studies with human platelets. *Blut* **54,** 193–200
38. Olgilvie, A. (1992) in *AP4A and Other Dinucleotide Polyphosphates* (McLennan, A. G., ed) pg. 357, CRC Press, Inc., Boca Raton, FL
39. Jankowski, J., Potthoff, W., van der Giet, M., Tepel, M., Zidek, W., and Schlüter, H. (1999) High performance liquid chromatographic assay of the diadenosine polyphosphates in human platelets. *Anal. Biochem.* **269,** 72–78
40. Lüthje, J., Baringer, J., and Ogilvie, A. (1985) Effects of diadenosine triphosphate (Ap3A) and diadenosine tetraphosphate (Ap4A) on platelet aggregation in unfractionated human blood. *Blut* **51,** 405–413
41. Ogilvie, A., Lüthje, J., Pohl, U., and Busse, R. (1989) Identification and partial characterization of an adenosine(5′)tetraphospho(5′)adenosine hydrolase on intact bovine aortic endothelial cells. *Biochem. J.* **259,** 97–103
42. Goldman, S. J., Gordon, E. L., and Slakey, L. L. (1986) Hydrolysis of diadenosine 5′,5″-P′,P″-triphosphate (Ap3A) by porcine aortic endothelial cells. *Circ. Res.* **59,** 362–366
43. Bollen, M., Gijsbers, R., Ceulemans, H., Stalmans, W., and Stefan, C. (2000) Nucleotide pyrophosphatases/phosphodiesterases on the move. *Crit. Rev. Biochem. Mol. Biol.* **35,** 393–432
44. Addison, W. N., Azari, F., Sørensen, E. S., Kaartinen, M. T., and McKee, M. D. (2007) Pyrophosphate inhibits mineralization of osteoblast cultures by binding to mineral, up-regulating osteopontin, and inhibiting alkaline phosphatase activity. *J. Biol. Chem.* **282,** 15872–15883
45. Kalya, S., and Rosenthal, A. K. (2005) Extracellular matrix changes regulate calcium crystal formation in articular cartilage. *Curr. Opin. Rheumatol.* **17,** 325–329
46. Levy-Litan, V., Hershkovitz, E., Avizov, L., Leventhal, N., Bercovich, D., Chalifa-Caspi, V., Manor, E., Buriakovsky, S., Hadad, Y., Goding, J., and Parvari, R. (2010) Autosomal-recessive hypophosphatemic rickets is associated with an inactivation mutation in the ENPP1 gene. *Am. J. Hum. Genet.* **86,** 273–278
47. Hirakawa, H., Kusumi, T., Nitobe, T., Ueyama, K., Tanaka, M., Kudo, H., Toh, S., and Harata, S. (2004) An immunohistochemical evaluation of extracellular matrix components in the spinal posterior longitudinal ligament and intervertebral disc of the tiptoe walking mouse. *J. Orthop. Sci.* **9,** 591–597
48. Okawa, A., Nakamura, I., Goto, S., Moriya, H., Nakamura, Y., and Ikegawa, S. (1998) Mutation in Npps in a mouse model of ossification of the posterior longitudinal ligament of the spine. *Nat. Genet.* **19,** 271–273
49. Flanagan, J. M., Sheehan, V., Linder, H., Howard, T. A., Wang, Y. D., Hoppe, C. C., Aygun, B., Adams, R. J., Neale, G. A., and Ware, R. E. (2013) Genetic mapping and exome sequencing identify 2 mutations associated with stroke protection in pediatric patients with sickle cell anemia. *Blood* **121,** 3237–3245
50. Jansen, S., Stefan, C., Creemers, J. W., Waelkens, E., Van Eynde, A., Stalmans, W., and Bollen, M. (2005) Proteolytic maturation and activation of autotaxin (NPP2), a secreted metastasis-enhancing lysophospholipase D. *J. Cell Sci.* **118,** 3081–3089
51. Saunders, L. P., Ouellette, A., Bandle, R., Chang, W. C., Zhou, H., Misra, R. N., De La Cruz, E. M., and Braddock, D. T. (2008) Identification of small-molecule inhibitors of autotaxin that inhibit melanoma cell migration and invasion. *Mol. Cancer Ther.* **7,** 3352–3362
52. Otwinowski, Z., and Minor, W. (1997) Processing of x-ray diffraction data collected in oscillation mode. *Methods Enzymol.* **276,** 307–326
53. Terwilliger, T. C., Adams, P. D., Read, R. J., McCoy, A. J., Moriarty, N. W., Grosse-Kunstleve, R. W., Afonine, P. V., Zwart, P. H., and Hung, L. W. (2009) Decision-making in structure solution using Bayesian estimates of map quality: the PHENIX AutoSol wizard. *Acta Crystallogr. D Biol. Crystallogr.* **65,** 582–601
54. Terwilliger, T. C., Grosse-Kunstleve, R. W., Afonine, P. V., Moriarty, N. W., Zwart, P. H., Hung, L. W., Read, R. J., and Adams, P. D. (2008) Iterative model building, structure refinement and density modification with the PHENIX AutoBuild wizard. *Acta Crystallogr. D Biol. Crystallogr.* **64,** 61–69
55. Zalatan, J. G., Fenn, T. D., Brunger, A. T., and Herschlag, D. (2006) Structural and functional comparisons of nucleotide pyrophosphatase/phosphodiesterase and alkaline phosphatase: implications for mechanism and evolution. *Biochemistry* **45,** 9788–9803
56. Emsley, P., Lohkamp, B., Scott, W. G., and Cowtan, K. (2010) Features and development of Coot. *Acta Crystallogr. D Biol. Crystallogr.* **66,** 486–501
57. Adams, P. D., Afonine, P. V., Bunkóczi, G., Chen, V. B., Davis, I. W., Echols, N., Headd, J. J., Hung, L. W., Kapral, G. J., Grosse-Kunstleve, R. W., McCoy, A. J., Moriarty, N. W., Oeffner, R., Read, R. J., Richardson, D. C., Richardson, J. S., Terwilliger, T. C., and Zwart, P. H. (2010) PHENIX: a comprehensive Python-based system for macromolecular structure solution. *Acta Crystallogr. D Biol. Crystallogr.* **66,** 213–221
58. Jansen, S., Perrakis, A., Ulens, C., Winkler, C., Andries, M., Joosten, R. P., Van Acker, M., Luyten, F. P., Moolenaar, W. H., and Bollen, M. (2012) Structure of NPP1, an ectonucleotide pyrophosphatase/phosphodiesterase involved in tissue calcification. *Structure* **20,** 1948–1959
59. Nikolic-Hughes, I., O'brien, P. J., and Herschlag, D. (2005) Alkaline phosphatase catalysis is ultrasensitive to charge sequestered between the active site zinc ions. *J. Am. Chem. Soc.* **127,** 9314–9315
60. Gijsbers, R., Ceulemans, H., Stalmans, W., and Bollen, M. (2001) Structural and catalytic similarities between nucleotide pyrophosphatases/phosphodiesterases and alkaline phosphatases. *J. Biol. Chem.* **276,** 1361–1368
61. Harahap, A. R., and Goding, J. W. (1988) Distribution of the murine plasma cell antigen PC-1 in non-lymphoid tissues. *J. Immunol.* **141,** 2317–2320
62. Rutsch, F., Vaingankar, S., Johnson, K., Goldfine, I., Maddux, B., Schauerte, P., Kalhoff, H., Sano, K., Boisvert, W. A., Superti-Furga, A., and Terkeltaub, R. (2001) PC-1 nucleoside triphosphate pyrophosphohydro-

lase deficiency in idiopathic infantile arterial calcification. *Am. J. Pathol.* **158,** 543–554

63. Pizzuti, A., Frittitta, L., Argiolas, A., Baratta, R., Goldfine, I. D., Bozzali, M., Ercolino, T., Scarlato, G., Iacoviello, L., Vigneri, R., Tassi, V., and Trischitta, V. (1999) A polymorphism (K121Q) of the human glycoprotein PC-1 gene coding region is strongly associated with insulin resistance. *Diabetes* **48,** 1881–1884
64. Meyre, D., Bouatia-Naji, N., Tounian, A., Samson, C., Lecoeur, C., Vatin, V., Ghoussaini, M., Wachter, C., Hercberg, S., Charpentier, G., Patsch, W., Pattou, F., Charles, M. A., Tounian, P., Clément, K., Jouret, B., Weill, J., Maddux, B. A., Goldfine, I. D., Walley, A., Boutin, P., Dina, C., and Froguel, P. (2005) Variants of ENPP1 are associated with childhood and adult obesity and increase the risk of glucose intolerance and type 2 diabetes. *Nat. Genet.* **37,** 863–867